The design and optimization of the down-lead system for a novel 400 kV composite pylon

Yin, Kai; Ghomi, Mohammad; Zhang, Hanchi; Silva, Filipe Miguel Faria da; Bak, Claus Leth; Wang, Qian; Skouboe, Henrik

Published in:
I E E E Transactions on Power Delivery

DOI (link to publication from Publisher):
10.1109/TPWRD.2022.3193562

Publication date:
2023

Document Version
Accepted author manuscript, peer reviewed version

The design and optimization of the down-lead system for a novel 400 kV composite pylon

Kai Yin, *Student Member, IEEE,* Mohammad Ghomi, Hanchi Zhang, Filipe Faria da Silva, *Senior Member, IEEE,* Claus Leth Bak, *Senior Member, IEEE,* Qian Wang and Henrik Skouboe

***Abstract*—This paper presents systematic research of a grounding down-lead design and its optimization for a novel Y-shaped composite pylon. A grounding down-lead inside the cross-arm is proposed as a potential grounding method. The transient response to lightning surges is modeled in PSCAD/EMTDC for a flash of lightning striking at the tip of the pylon. Aiming at the characteristic of the pylon structure, we propose theoretical formulas to calculate the surge impedance of the inclined down-lead circumscribed by composite materials. Besides, potential multi-factors affecting BFR such as the configuration as well as the length of the down-lead, the pylon span, the dielectric constant of the filling material, the electromagnetic propagation speed of the lightning, and the capacitances between down-lead and phase conductors are investigated, after which the grounding lead system of the pylon and filling materials are determined. Afterwards, the applicability of the multi-down-lead system to increase critical current (I_c) is discussed considering the lightning current capacity and the corona generation. Finally, we verify the insulation of the down-lead system. Compared with that of traditional Eagle and Donau towers, the backflashover rate (BFR) of the Y-shaped pylon with an optimized down-lead system is lower than that of traditional ones.**

***Index Terms*—BFR, composite pylon, surge impedance, optimization, dielectric constant.**

I. Introduction

The ongoing expansion of renewable energy generation, such as offshore wind and solar power, raises a massive demand for new transmission towers [1-3]. Due to its lower economic and environmental impacts, composite material should be an alternative to the metal used in a lattice transmission tower [4]. According to the project of 'Power Pylons of the Future', a composite pylon that has a 'Y' shape with an integrated cross-arm without insulator strings is a promising solution [5]. Compared with traditional transmission towers, the compact design of the pylon configuration can reduce line corridor areas and the use of steel, decreasing the cost of transportation and assembly [6]. Meanwhile, this new type of pylon is positively dominant with respect to visual impact [7].

Lightning is the main factor affecting the safe and reliable operation of transmission lines. Therefore, evaluating the lightning protection performance of composite pylon has an essential significance. The backflashover rate (BFR) and shielding failure flashover rate (SFFOR) are critical evaluation criteria for the lightning performance of transmission towers. However, to date, there are just a few scientific works on SFFOR of the fully composite pylon. T. Jahangiri *et al.* [8] studied the strengths and weaknesses of the preliminarily assigned shielding angle for the pylon. They used the revised electro-geometric model (EGM) to calculate the shielding failure rate. The maximum shielding failure current that was determined referred to multiple standards. The research showed that transmission lines supported by the Y composite pylon have a lower striking probability due to its compact pattern when compared with the two conventional steel towers considered in this paper, and a higher critical current of shielding failure. Due to the negative protecting angle of -60° adopted by the Y composite pylon, the theoretical SFFOR of the composite pylon is close to zero. The shielding failure rate (SFR) of the Y shaped pylon is no more than 0.009 flashes/100 km-year [8]. In summary, the theoretical calculation for this new pylon shows an almost perfect evaluation in the point of shielding failure. Subsequently, Wang et al. [9] conducted the relevant test. The spatial shielding failure probability around the tower was calculated based on the ratio of discharge paths recorded in the test. The test results verified the feasibility of EGM in the lightning performance evaluation of the fully composite pylon and confirmed that the special negative shielding angle in the new composite tower provides good lightning shielding performance [9]. Although this research was based on scale model which has limitations to simulate the real case because the facility and space limitations and degree of air ionization is not changed linearly with the scale ratio, scale model is still meaningful for lightning performance investigation due to the similarity of the long gap discharges in the laboratory with the final stage of natural lightning. The scale-test has a very limited deviation with the revised EGM results and therefore is being corroborated analytically. It provides a valuable reference for lightning shielding performance evaluation of the novel composite tower.

Actually, the BFR depends on the structure of the pylon and the down-lead configuration. The BFR of the composite pylon

Manuscript received October XX, 2020; revised XX, 2020 and XX, 2020; accepted XX, 202X. Date of publication XX, 202X; date of current version March XX, 202X. *(Corresponding author: Hanchi Zhang)*

K. Yin, M. Ghomi, H. Zhang, F. F. da Silva, C. L. Bak, and Q. Wang are with the Department of Energy, Aalborg University, Aalborg 9100, Denmark (e-mail: kyi@energy.aau.dk; mhg@energy.aau.dk; hazh@energy.aau.dk; ffs@energy.aau.dk; clb@energy.aau.dk; qiw@energy.aau.dk).

H. Skouboe is with the BYSTRUP Architecture Design Engineering, KØbenhavn Ø 2100, Denmark (e-mail: hs@bystrup.dk).

Color versions of one or more of the figures in this paper are available online at http://ieeexplore.ieee.org.

Digital Object Identifier 10.1109/TPWRD.2017.2716383

is serious lacking systematic research due to its unusual configuration and undefined down-lead system. Unlike traditional transmission towers, the new pylon body has more compact pattern and is entirely composed of non-conductive composite material, and the integration of insulators in a form of uni-body cross-arm replace the conventional suspension insulators. The lower height of the pylon means the higher capacitance of the downlead to the ground. The shield wire and three phase conducting wires are arranged along the cross-arms of the double-circuit composite pylon as shown in Fig. 1. The special features of the phase arrangement result in non-equalizing induced voltage and biased flashover probability between the upper phase conductor to the shield wire. Secondly, the electromagnetic transient (EMT) modeling for the metal tower body and downlead system is totally different. In the determination of the surge impedance, the lattice structure of the traditional tower is always treated as a cone. The bracing as well as the metal cross-arm can be expressed by distributed constant lines. While for the composite tower, the downleads consist of cylinders at an angle of 30° to the horizontal. Thirdly, two shield wires mounted on the tips of composite pylon are not directly connected, and the mutual coupling effect on the lightning performance is also unclear. In addition, traditional steel frames are not covered with insulating materials, nevertheless, the presence of composite material around the downlead will changes its capacitance as well as the mutual capacitance to the phase conductors. The influence of the composite materials on the electrical parameters of the down-lead cannot be analyzed with the resort of conventional simulation model or formulas. Thus, those structure and electrical differences need to be fully considered in the research of the BFR of the Y-shaped pylon.

Significantly, there is no path for providing ground potential for shield wires in the initial design. To date, a suitable technical solution for the grounding system of this new pylon has not yet been determined. Thus, the first step to obtain the BFR is to identify effective grounding methods. In light of the reality of the 'Y' shaped composite pylon, we propose two different methods for grounding the down-lead. The first method is a bare grounding conductor going down through the Fiber-Reinforced Plastic (FRP) cross-arm tube and the pylon body. Another technique is a grounding lead going down outside the cross-arm and the pylon body. These two methods are referred to as the internal grounding and the external grounding, respectively. For external grounding, this method has only been applied for a newly designed 110 kV semi-composite tower in China [10]. It reported that both BFR and SFFOR of that tower showed acceptable levels. However, the configuration of the tower should guarantee enough safety distance between the vertical down-lead and the tower body to avoid arc occurring between down-lead and phase conductors, and this design increases the complexity and difficulty of installation. For the Y shaped pylon, increasing the lead to phase conductor distance means an increase in the line corridor areas, leading to a larger right-of-way and a bigger visual impact, which limit the advantage of the pylon structure. If the internal grounding technique is used as the grounding method, the structure of the pylon does not need to be changed and those issues regarding the external grounding mentioned above can be avoided. However, the research about the feasibility of down-lead going through the pylon body is absent. Therefore, the insulation coordination and capacity of conducting a lightning current in an internal down-lead is investigated in this paper.

In this paper, we propose a metal lead going down through the Fiber-Reinforced Plastic (FRP) cross-arm and the pylon body as a grounding system. The surge impedance of the down-lead is determined through the image method [11]. Then the PSCAD/EMTDC is employed to investigate the transient overvoltage response when lightning strikes on the shield wire. Afterward, we investigate multi-factors affecting the lightning performance and determine the filling materials and cross-section area of the down-lead with regarding the current capacity. The feasibility of multi-down-lead system is discussed from the perspective of surge impedance and corona effect. Finally, the lightning performance of the optimized pylon is systematically evaluated and contrasted with traditional Donau and Eagle towers.

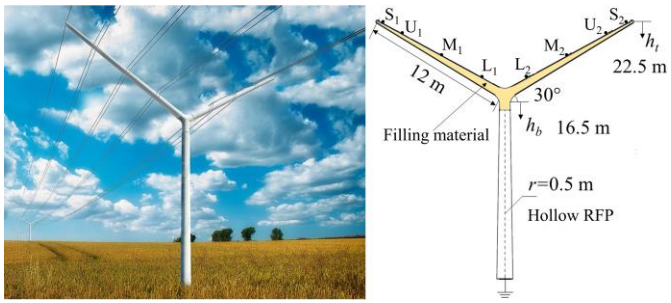

Fig. 1 Concept map of the composite 'Y' pylon. S refers to shield wires. U, M, and L refers to upper, middle, and lower phase conductors.

II. Pylon Model Build

In order to calculate the lightning transient responses, the equivalent circuit of the pylon, which directly affects the accuracy of results, needs to be determined first. Figure 1 shows the concept map of the double circuit 400 kV fully composite pylon [3], with the pylon adopting a novel unibody cross-arm with an inclination angle of 30°. The height (h_t) of this tower is 22.5 m, which is considerably lower than that of traditional ones with the same voltage level [12]. The height (h_b) and the external radius of the vertical column part of the tower body are 16.5 m and 0.5 m, respectively. The length of the cross-arm is 12 m. The integrated insulators in the form of unibody cross-arm replace the insulator strings used in traditional lattice towers. Meanwhile, clamps are mounted on the cross-arms, and Aluminum Conductor Steel-Reinforced (ACSR) conductors in a duplex bundle are used. According to IEC 60071-1 [13] and CIGRE TB.72 [14], the required phase-to-phase and phase-to-shield wire air clearances on the unibody cross-arm are 3.68 m and 2.8 m, respectively [15]. Two separated bare conductors connected with the shielding wires are arranged through the pylon cross-arm and body. There is no connection between two down-lead, and we refer this configuration as 'II' frame. The pylon mast is a hollow FRP

according to the initial design, while the cross-arm is filled with composite materials between the sheath and down-lead. The initial design of the span between pylons is 250 m.

PSCAD/EMTDC is employed to obtain the overvoltage at the shield wires when struck by lightning flashes. A double circuit transmission line with seven pylons is modeled as the base of the simulation with a lightning flash hitting on the tip of the middle pylon. Bergeron model with a steady-state frequency of 10 MHz is used for modelling the lines. The coupling effect of both the inclined and vertical parts of downleads have also been taken into consideration. The equivalent circuit of the down-lead system is exhibited in Fig. 2 (a). Where M_{Li} (i=1 to 5) is the mutual inductance.

A. Surge impedance of the down-lead

The surge impedance of the down-lead system is key in determining the lightning transient overvoltage [16]. The ground system mainly consists of the sloping down-lead inside the cross-arm, vertical down-lead inside the tower body and footing resistance. Due to the inclination characteristics of the cross-arm and the unique configuration, there are no empirical formulas available to calculate the surge impedance of the down-lead inside the cross-arm. Besides, the previous work reported that if the cross-arm is hollow, the surface E-field of the down-lead would exceed the maximum admissible E-field magnitude [17, 18]. Therefore, filling materials for cross-arm, which are adopted to curb the electric-field distortion, also need to be considered in the determination of the surge impedance. Here, we initially choose the FRP as the filling material. Inspired by a multistory tower model [19], the down-lead inside the cross-arm can be divided into 4 segments, The inductance and capacitance corresponding to each segment are obtained by integration as (1) and (2).

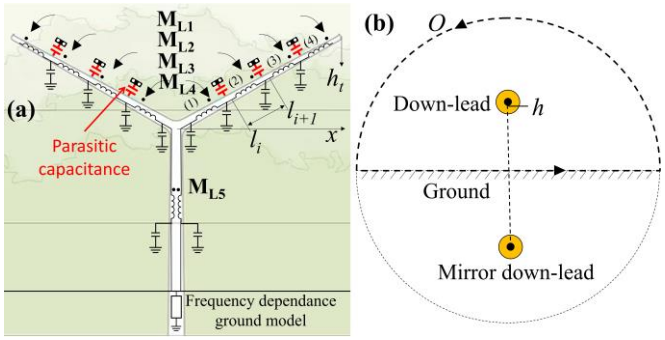

Fig. 2 The schematic of the (a) equivalent circuit model and (b) the integral path to simulate the surge impedance of the down-lead segment.

$$L=\int_{l_1'}^{l_2'}\frac{1}{2\pi}\left(\mu_1\ln\frac{b}{a'}\frac{2h-a'}{2h-b}+\mu_0\ln\frac{2h-b}{b}\right)dx \quad \text{H} \qquad (1)$$

$$C=\int_{l_1'}^{l_2'}\frac{2\pi}{\frac{1}{\varepsilon_1}\ln\frac{b}{a'}\frac{2h-a'}{2h-b}+\frac{1}{\varepsilon_0}\ln\frac{2h-b}{b}}dx \quad \text{F} \qquad (2)$$

Where l, h, and b are the length, height, and radius of the cross-arm segments. a is the radius of the down-lead. $a'=a/\cos 30°$ and $l'=l\cos 30°$. μ_1, ε_1 are the permeability (approximated as vacuum permeability μ_0) and the dielectric constant of the filling materials ($\varepsilon_1=2.64\varepsilon_0$) [5].

To verify the surge impedance of the down-lead segments, the COMSOL RF-module is employed. Assuming perfect conductors and a lossless air region, the surge impedance can be obtained by calculation of the ratio of the conductor voltage to its current. The voltage V can be evaluated as an integral of the electric field $\boldsymbol{E}$ along the direct line from down-lead to ground (3), and the current I is an integral of the magnetic field $\boldsymbol{\Psi}$ along a closed loop O of the down-lead (4). The cross-section schematic of integration path is shown in Fig. 2(b), and the electric field distribution of the down-lead is exhibited in Fig. 3. The comparison between the theoretical values and simulation values are shown in Table I. The largest error is about 3.14%.

$$V=\frac{1}{2}\int_{-h}^{h}\boldsymbol{E}dx \qquad (3)$$

$$I=\oint_{O}\boldsymbol{\psi}dx \qquad (4)$$

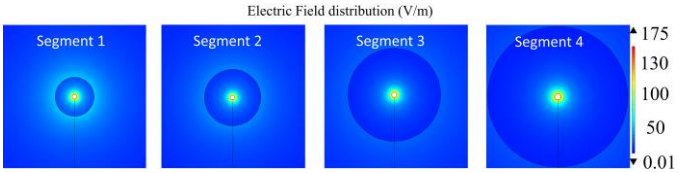

Fig. 3 The electric field distribution of down-lead segments.

TABLE I: COMPARISON OF THEORETICAL AND SIMULATED VALUES

	Segment 1	Segment 2	Segment 3	Segment 4
Simulation values	434.03 Ω	421.54 Ω	408.34 Ω	396.34 Ω
Theoretical values	420.80 Ω	408.84 Ω	397.05 Ω	388.42 Ω

The velocity of the lightning propagation in each segment can be obtained from the inductance and capacitance.

$$v=1/\sqrt{LC} \qquad (5)$$

The surge impedance of vertical part of down-lead is generally suggested as (6) [19, 20]

(6)

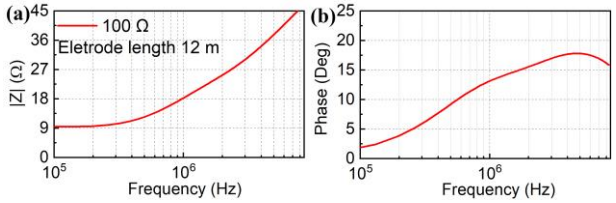

Fig. 4 The impedance behavior includes (a) magnitude and (b) phase of the vertical electrodes buried in uniform soil.

B. Footing resistance

The footing resistance of a pylon is primarily influenced by the shape of electrodes, soil conditions and the lightning current amplitude. The concentrated ground electrode consists of four rods with each length of 3 meters in series connection and they are mounted on the bottom of the pylon body. The uniform soil model is considered as ground model [21]. Take the soil situation in Denmark as an example, 100 Ω·m is suggested as a conservative value for soil resistance ρ_0 [22]. The input impedance of tower-footing can be obtained by the electrical field integral equation which can be solved by the method of

moment [21]. The magnitude and phase of the input impedance are shown in Fig. 4. Additionally, for comparison purpose, all towers adopt the same grounding system.

C. Lightning parameters

Herein, the CIGRE lightning current waveform was employed to investigate the transient response of the Y shaped pylon. In practice, the front time of lightning flashes is not constant. In the procedure of simulating I_c, the 0.2-10 μs front time T_f is taken into consideration to illustrate the results are suitable for different T_f. Reference [24] showed that the tail duration of lightning current has an insignificant effect on the transient voltage, so the tail time T_t is set to a constant of 77.5 μs. The correlation between the lightning steepness (S_m) and its crest current I_F follows [25]:

$$S_m=1.4I_F^{0.77} \tag{7}$$

The surge impedance of the lightning current discharge channel is set to 1000 Ω [16, 23].

D. Intersection capacitances

Due to the unique grounding system, the insulation distance between the phase conductor and the down-lead is much shorter than in traditional lattice ones. Meanwhile, the isolating dielectric with a higher dielectric constant will result in large parasitic capacitances. Thus, the parasitic capacitances between down-lead and phase conductors (called the intersection capacitance in this paper) as well as the capacitances between the inclined down-leads should be taken into consideration in the equivalent circuit of the pylon. To obtain the capacitances, the finite element method (FEM) based software COMSOL is employed for 3D modeling. A non-zero potential is applied on one conductor, while other phase conductors and down-leads, were set to zero potential. Then we can get capacitances through the Maxwell capacitance matrix (Table II).

TABLE II: INTERSECTION AND MUTUAL CAPACITANCES

Capacitance(pF)	Upper phase to down-lead	Middle phase to down-lead	Lower phase to down-lead
	46.17	51.41	50.43

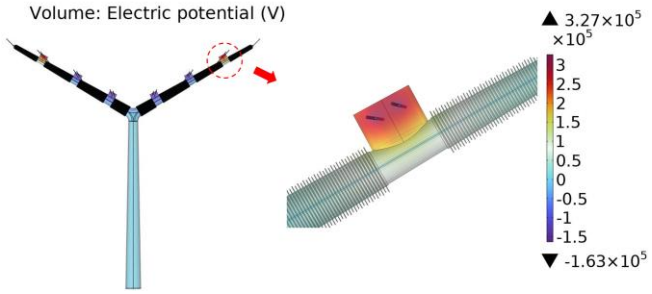

Fig. 5 (a) The potential distribution of downleads inside cross-arms applying 400 kV crest phase voltage.

E. Mutual coupling effect between two downleads

The mutual coupling in the multi-conductor system should be taken into consideration. The mutual coupling among horizontal phase conductors is considered in PSCAD by default once the spatial position of the phase conductors is determined. Two downleads can establish the coupling through the mutual impedance. For two downlead system, given the current τ on the conductor, the voltage V_1 and V_2 of conductors are [25]

$$\begin{aligned} V_1&=Z_{11}\tau_1+Z_{12}\tau_2 \\ V_2&=Z_{21}\tau_1+Z_{22}\tau_2 \end{aligned} \tag{8}$$

Where Z_{11} and Z_{22} are the down-lead self-impedance, while Z_{12}=Z_{21} is the coupling impedance, which can be obtained by mutual capacitances and inductances. By the means of COMSOL, mutual capacitances can be simulated in Maxwell capacitance matrix and mutual inductance obtained in Coil parameters. Figure 5 shows the potential distribution derived when calculating the matrix.

F. Flashover criterion

The leader progression model (LPM) has been widely applied in the judgment of flashover occurrence [26]. The leader propagation characteristics are obtained by practical experiments for air gaps or insulators. The leader propagation speed of lightning impulse voltage in the function of flashover time is given by (9) according to the CIGRE WG C4.23 [27].

$$\frac{dz}{dt}=ku(t)\left(\frac{u(t)}{D-z}-E_0\right). \tag{9}$$

Where z is the length of the leader, $u(t)$ is the voltage at the air gap, D is the length of insulation, E_0 is the threshold electric field of leader progression and k is the factor of leader progression speed. E_0 and k are related to the type of the insulators and the polarity of the lightning impulse voltage, which are obtained from experiments. Due to the similar material components and insulator configuration, the flashover characteristics along the composite insulator can be regarded as that of a post insulator [28]. The k and E_0 for negative discharge are recommended to be 1.0×10^{-6} m^2/V^2/s and 670 kV/m [27].

When the leader progresses continually until the remain gap distance is less than h_f, the leader will jump, resulting in gap breakdown. The jump threshold h_f is given by [29]

$$h_f=3.89/\left(1+3.89/D\right) \tag{10}$$

G. BFR calculation

For 220 kV and above transmission lines, the phase voltage has a considerable impact on the lightning performance and therefore, the voltage phase and polarity when lightning strikes should be considered. The flashover judgment between upper phase and shielding wire can be expressed as

$$U_{\text{flashover}}=U_i+U_p \tag{11}$$

$$U_p=\frac{400\sqrt{2}}{\sqrt{3}}\sin(100\pi t+\varphi) \tag{12}$$

Where U_i is the voltage between the phase conductor and shield wire. U_p is the phase voltage. Practically, the probability density function of front, tail duration, and amplitude of lightning current can be approximately expressed by a lognormal distribution as (13) shows. Thus, the incremental T_f with constant T_t is closer to the actual situation to investigate the BFR.

$$f(x)=\frac{1}{\sqrt{2\pi}\beta x}e^{-\frac{1}{2}\left(\frac{\ln(x/M)}{\beta}\right)^2} \tag{13}$$

The mean value μ of the lightning parameter can be determined by the two coefficients M and β. The statistical median values of the T_f and T_t are 3.83/77.5 μs, 31.1 kA for I_c [25].

$$\mu = Me^{\frac{\beta^2}{2}} \tag{14}$$

In this research, critical current I_c under varied T_f is investigated, and the I_c considers the influence of the phase voltage. P_c is the cumulative distribution function of (13) that the stroke current from 0 to I_c. The BFR can be obtained by

$$BFR = 0.6 N_L \int_0^{\infty} f(T_f)\left[1 - P_c(I_c)\right] dT_f \tag{15}$$

Where $f(T_f)$ is the probability of a lightning current with a T_f. N_L estimates the number of strikes to the line per year per 100 km, which can be calculated according to (16) [25].

$$N_L = \frac{N_g}{10}(28 h_t^{0.6} + W) \tag{16}$$

Where W is the horizontal width between two shielding wires. The worst N_g, which refers to the lightning flash density in Denmark, for the last decade is equal to 1.39 flashes/km^2·year [30, 31].

In practical calculation, the first step is to determine the discrete T_f as well as the corresponding I_c. In general, when T_f exceeds 10 μs, the corresponding backflashover probability is less than 10^{-5} [25], which has little impact on the total BFR. Thus, I_c considering a number of 50 discrete T_f values (in the range of 0.2-10 μs and an increment ΔT of 0.2 μs) has been used. Then the probability of T_f and I_c can be obtained by (12). The corresponding probability of each T_f is $f(T_f)\Delta T$. Finally, the total BFR considering T_f range can be obtained (15).

$$BFR = 0.6 N_L \sum_{i=1}^{50} \left[f(T_f)\Delta T \left(1 - P_c(I_c)\right)\right] \tag{17}$$

III. Influence Factors on BFR

A. BFR of initial grounding design

The PSCAD simulation shows that the critical lightning current I_c with a CIGRE lightning current waveform (3.83/77.5 μs) able to cause flashover is 132 kA. BFR is estimated to about 0.0238 times per year per 100 km, which is nearly quadruple of the BFR for 400 kV lattice Donau tower (Table III). For strong lightning activity areas, the BFR will linearly increase along with N_g. It will limit the application scope for this transmission pylon. Therefore, the ground system design should be optimized to increase its I_c.

B. Pylon span

Subsequently, we focus on the influence of the pylon span on the transient overvoltage. The pylon span varies from 200 m to 400 m, and a set of lightning currents with different T_f and a constant magnitude of 31.1 kA (3.83/77.5 μs) are striking on the top of the pylon to investigate the overvoltage waveform. The voltage waveform stressed on the cross-arm (U_L) with different pylon spans is plotted in Fig. 6 (a)-(c). We can find that there are obvious drops on the tail duration. Meanwhile, a slight drop can be observed at the lightning front and the drop time is exactly twice span travel time T_s. The pylon span has little impact on the crest voltage of U_L but the tail duration, which can affect the leader propagation speed, along with the I_c, as shown in Fig. 6 (d). It can be deduced that the reflection from the adjacent towers will reform the tail shape. The shorter pylon span makes the travel time shorter, shortening the tail time of U_L and shifting its crest to an earlier moment. The shorter span can increase the I_c but the effect is limited. Considering the I_c and the mechanical load-bearing capability, the pylon span follows the previous setting.

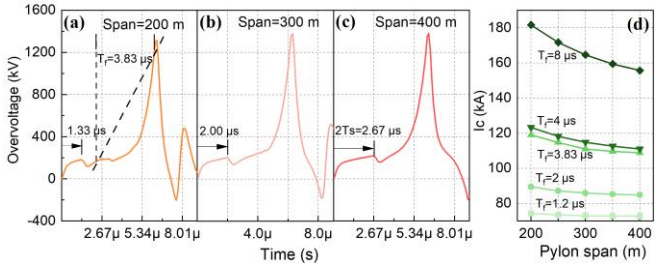

Fig. 6 (a)-(c) The transient overvoltage of Y shaped pylon with different transmission span when lightning strikes on the top of the pylon. (d) The I_c of the Y shaped pylon with different pylon span.

C. Length of the down-lead

The effect of the length of the down-lead on I_c is considered. The U_L corresponding to the down-lead length of 26 m, 28 m, and 30 m with a 31.1 kA (3.83/77.5 μs) lightning current striking are shown in Fig. 7 (a) and corresponding I_c is shown in Fig. 7 (b). The results show that with the decrease in the length of the down-lead, the lightning travelling time from tower top to tower bottom (T_p) decreases, U_L correspondingly decreases and the crest advances. This means the T_p influence on the overvoltage and the span effect in a certain range can be ignored for this kind of pylon. However, the shortening of down-lead is restricted by the tower structure. Therefore, to further improve the lightning performance, other characteristics of the ground system should be considered.

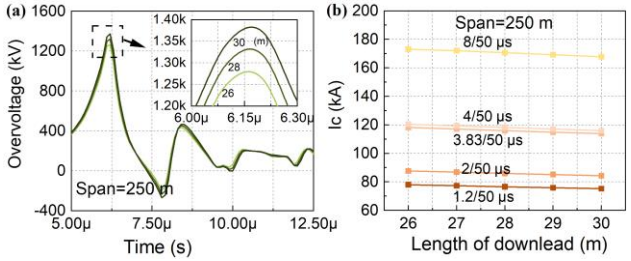

Fig. 7 (a) The waveform of U_L with different down-lead length with lightning strikes on the top of the pylon. (b) The critical current (I_c) as a function of the length of the down-leads with varied T_f.

D. Filling materials

As mentioned before, the cross-arm tube and pylon body are filled with composite materials. The dielectric constant of filling composites determines the mutual surge impedance and the phase-to-downlead capacitance, and T_p. These factors affect the lightning performance of the pylon, and they are studied to pave the way to a further optimization of the grounding system.

1) Intersection capacitance effect

Filling materials in the cross-arm with different dielectric constants would result in different intersection capacitances. Here, we investigate the effect of the intersection capacitance on the overvoltage level. The control variate method is adopted, and we assume that the surge impedance of the down-leads is uninfluenced by the dielectric constant of filling material firstly. There are two groups of modeling, one is a set of lightning currents with different T_f striking on the top of pylons

under the intersection capacitances considered, and the other group does not consider the intersection capacitances. The simulation results reveal that the intersection capacitance has little effect on the generated overvoltage.

2) Lightning velocity and surge impedance

The stroke current propagation speed in the down-lead conductor is also another factor affecting the transient overvoltage. The dielectric constant of the filling materials directly affects the lightning propagation time and surge impedance of down-lead in cross-arms. There is a contradiction that reducing the dielectric constant will decrease the propagation time, which is positive for lightning protection. However, a decrease in dielectric constant also decreases the mutual electromagnetic effect and increases the surge impedance, which is negative for lightning performance. The surge impedance and propagation time change along with dielectric constant oppositely as shown in Fig. 8 (a). The presence of the filling material inside the cross-arm diverts and delays a fraction of the surge at the cost of the increasing surge traveling time. Thus, we need to identify which factor is more dominant with different *k*. We found that I_c remains a stable status with the dielectric constant increasing, and regardless of T_f (Fig. 8 (b)). Thus, the propagation time extension caused by varied *k* offsets the effect of the decreasing the surge impedance, and I_c is not affected by material properties.

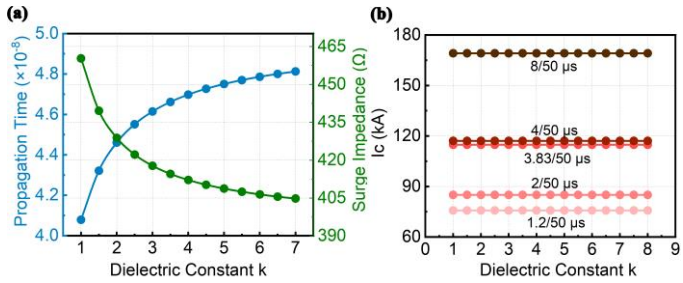

Fig. 8 (a) The lightning propagation time and surge impedance as a function of dielectric constant of filling materials. (b) The I_c changes with dielectric constant with varied T_f.

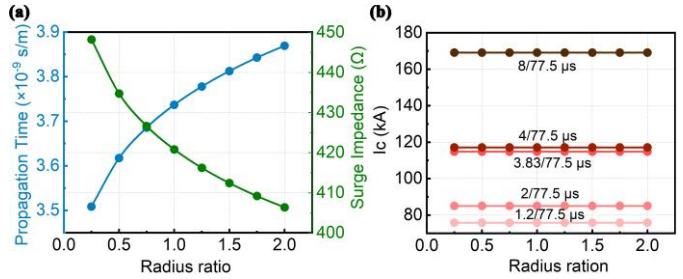

Fig. 9 (a) The lightning propagation time and surge impedance as a function of the ratio radius. (b) The I_c changes against the ratio radius with varied T_f.

3) The radius of the composite cross-arm

The radius of the cross-arm determines the insulation strength between the down-lead and the upper phase conductor. In the initial design, the cross-arm is cone shape with the top radius of 0.125 m and the bottom radius of 0.4 m. Taking the initial design as a standard, the radius is scaling at a certain ratio range from 0.25 to 2, and the corresponding propagation time and surge impedance of the segment (1) cross-arm are shown in Fig. 9. We can conclude that the radius increases the propagation time and decreases the surge impedance simultaneously, but the net effect also can be neglected on the I_c. The radius parameter of the composite cross arm has an insignificant impact on I_c. In other words, the radius of the cross-arm can be adjusted to guarantee there is no puncture between the down-lead and the upper phase conductor while I_c without being affected. Therefore, the filling material puncture is not considered in this paper.

IV. Optimization of Down-Lead

A. Down-lead ampacity verification

According to the conclusion that the dielectric constant of the filling materials almost has no impact on the critical current with lightning striking. Therefore, the selection of the filling materials should mainly emphasize on the thermal stability and insulating level to avoid the partial discharge and thermal erosion. Crosslinked polyethylene (XLPE) has good insulation, chemical resistance, and thermo-mechanical performance at high temperature with low dielectric loss and low the density, which is selected as the filling material [32]. Meanwhile, any non-corrosive metal or alloy with high ability of current conduction can be used as down lead materials. Here, we take copper as example to verify whether the downlead parameters are reasonable to meet the thermal and electrical requirements. The down-lead with filling materials can be approximately regarded as a cable. Due to the extremely short duration of lightning current, its current capacity can be estimated by referring to the adiabatic short-circuit current capacity for a single cable [33]. The maximum withstand current is I_{AD}.

$$I_{AD} = KA\sqrt{\ln\frac{\theta_f+\delta}{\theta_i+\delta}\Big/ t_{\mathrm{d}}} \tag{18}$$

Where t_{d} is the duration of the lightning current. The mean time of the lightning is 200 ms [25]. *K* is a constant depends on the downlead material and recommended to be 226 $As^{1/2}/mm^2$ for copper [33]. θ_f is the instantaneous maximum withstand temperature of XLPE about 250 ℃ [34], θ_i is the environmental temperature about 70 ℃ [35]. δ is the reciprocal of resistance temperature coefficient. *A* is the cross-sectional area of downlead core (mm^2). Considering the worst case that a flash lasts for a whole lightning duration, I_{AD} can be obtained as 331 kA. The corresponding probability that the lightning stroke current exceeds this level is less than 8.7×10^{-6} flashes/100km-year. We believe that the design of the copper downlead meets both thermal and electrical requirements.

B. Optimization of the vertical down-lead

1) The multi-down-lead system

For the vertical grounding system, two separated down-leads can be linked directly to form an entity. At this time, the surge impedance of the linked down-lead will decrease [25]. This configuration can be represented as 'H' frame. If multiple down-leads are interconnected as multi-strand conductors by wire fittings, the total surge impedance of the down-lead can be reduced further [36]. The whole impedance $Z_{T,n}$ can be expressed by the average of the self-impedance $Z_{T,kk}$ and mutual surge impedance $Z_{T,kl}$ ($k \neq l$) (19).

$$Z_{T,n} = \frac{1}{n}(Z_{T,11} + Z_{T,12} + \cdots Z_{T,1n}) \tag{19}$$

$$Z_{T,kl} = 60(\ln\frac{2\sqrt{2}h}{S_{kl}} - 1) \tag{20}$$

Where S_{kl} is the distance between the k^{th} and l^{th} cylinders. By simplifying, $Z_{T,n}$ can be rewritten as a function of the equivalent radius r_e as (21):

$$Z_{T,n} = 60(\ln\frac{2\sqrt{2}h}{r_e} - 1) \tag{21}$$

Where h is the height of the vertical down-leads, n is the number of down-leads in the vertical ground system and a is the radius of a single down-lead. The vertical conductors are arranged as regular polygons around the inner surface of the composite body. That means the inner radius of the regular polygon conductor system is a constant R (Fig. 10 (a)). The equivalent radius of the multi-conductor is given by (22).

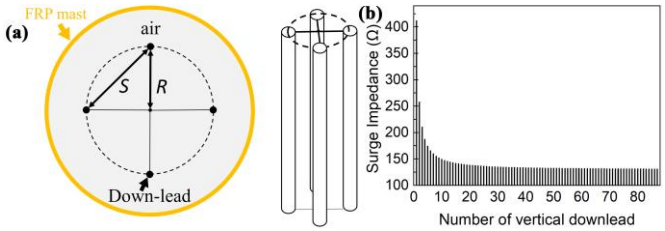

Fig. 10 (a) The configuration of vertical down-leads from overhead view and front view. (b) The surge impedance of vertical down-lead system as a function of the number of the down-leads.

$$r_e = (2R)^{\frac{n-1}{n}} a^{\frac{1}{n}} \left(\prod_{i=1}^{n-1} \sin\frac{\pi i}{n}\right)^{\frac{1}{n}} \tag{22}$$

In fact, the core of solving the surge impedance of the multi-conductor system is to determine the equivalent radius of the multi-down-lead system. According to the equivalent radius (r_{eq}) formula of bundle conductor (23), r_{eq} is expressed as [37]. The r_{eq} is numerically equal to r_e.

$$r_{eq} = \sqrt[n]{aS_{11}S_{12}\cdots S_{1n}} \tag{23}$$

As the number of vertical down-leads increases, the $Z_{T,n}$ decreases sharply at first and then gradually reaches saturation as Fig. 10 (b) shows. If n increases infinitely (n>>[π/arcsin(r/L)]), and R>>a, the vertical grounding system becomes a metal cylinder.

$$\sqrt[n]{\left(\prod_{i=1}^{n-1} \sin\frac{\pi i}{n}\right)} \approx 0.5 \tag{24}$$

Thus, r_e infinitely approaches R+a. Taking the parameters in this manuscript as an example, the calculation error compared with the (25) is 0.87 %.

$$Z_{T,n} = 60(\ln\frac{2\sqrt{2}h}{R+a} - 1) \tag{25}$$

2) Simulation verification

To verify the equivalent radius of the down-lead system, we use COMSOL RF-module to simulate the surge impedance of the down-leads. The process of simulation setting is same as the simulation for surge impedance of down-lead in section II A.

In the geometry design, conductors are located at the vertexes of regular polygons of which the circumscribed circle radius is 0.5 m. Then, the integral path should be defined. The surge impedance is analyzed finally.

The top view of the electric field distribution of the down-lead system is shown in Fig. 11 (a) with a 3000 kV transient overvoltage applied. Figure 11 (b) and (c) show the simulated and calculated values for the equivalent radius and surge impedance, and the biggest error is 2.87 %.

The I_c against the number of the down-leads is shown in Fig. 11 (e), assuming the impedance has not been affected by corona.

3) Corona effect

The thermal stability and the partial discharge have been fully verified during the selection of the down-lead and filling materials. Thus, there is no internal discharge inside the cross-arm. But for the vertical down-lead, the surface of the steel is explored to the air. When a large lightning current goes through the down-lead, there is a high electric potential, which is prone to generate corona at the top of the vertical down-lead. The corona discharge will produce nitrogen oxides and ozone [38], which can react with moisture in the air to form strong

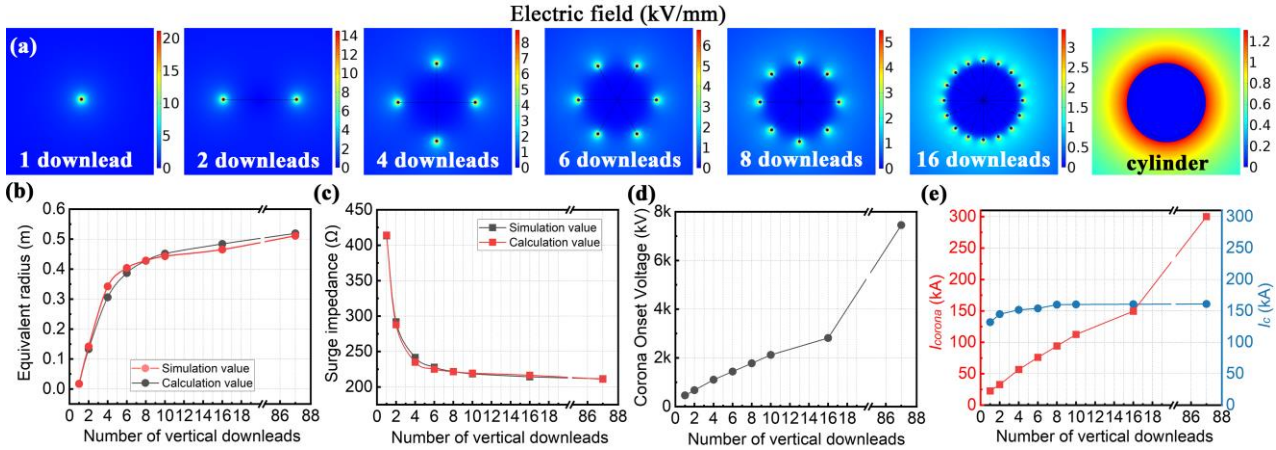

Fig. 11 The top view of the electric field distribution of the vertical-downleads with 3000 kV applied voltages. The theoretical value and simulated value of the (b) equivalent radius and (c) surge impedance. (d) The corona onset voltage for the multi-conductor system, and (e) the critical lightning current to induce the corona (I_{corona}) and I_c at the triple conjunction point of the multi-down-lead system.

acid mist inside of the pylon mast, posing potential erosion and aging risks to composite materials. Although the likelihoods of such are not presently well defined, in the design of the down-lead system, the risk from corona should be avoided. Thus, the corona onset voltage of the vertical down-lead is studied.

The surface of the corona threshold electric field E_{co} should be determined, which is influenced by multi-factors [39]. CIGRE Brochure given the E_{co} (kV/mm) for metal cylinder based on experiment data in standard atmospheric pressure [27].

$$E_{co} = 2.3(1+\frac{1.22}{a^{0.37}}) \tag{26}$$

For the vertical down-lead with radius a=17.5 mm, the corona onset electric field is 3.27 kV/mm. Then, by the means of Finite Element Method, the critical onset voltage able to make the surface field strength of the down-lead reaching the voltage of corona field strength can be simulated (Fig. 11 (d)). As the number of the down-lead increases, the surface electric field weakens for the same voltage. Combining with PSCAD/EMTDC, the critical lightning current induced the corona (I_{corona}) at the triple conjunction point is shown in Fig. 11 (e). When the number of the down-leads less than 18, I_{corona} is lower than I_c. At this moment, the I_{corona} represents the largest allowable lightning current for pylon safety operation. It can be clearly seen that the corona phenomenon seriously restricts the advantages of the composite pylon on the lightning performance. When the pylon mast is replaced by the steel cylinder with radius of 0.5 m, the corresponding I_{corona} simulated by EMT is more than 300 kA, and there is almost no probability of corona. Thus, the Y shaped pylon with steel cylinder mast has enough surficial electrical insulation strength to avoid the potential corona risk.

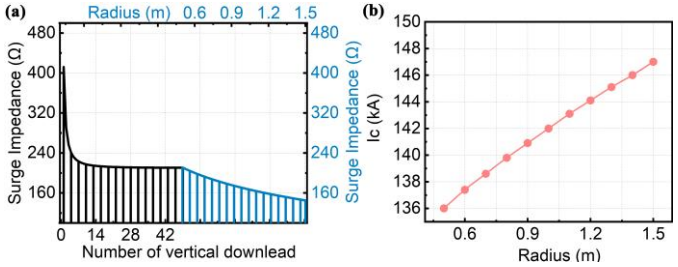

Fig. 12 (a) The surge impedance of multi-conductor system as a function of number of down-leads, and the surge impedance of the steel mast as a function of radius. (b) I_c (3.83/77.5 μs) corresponding to different radius.

4) Radius extension of the steel mast

For pylon with steel cylinder of 0.5 m, I_c (3.83/77.5 μs) is approximately 162 kA. The surge impedance of the vertical mast would be further decreased by expanding its radius (Fig. 12 (a)). When the radius of the mast increases to 1.5 m, the I_c (3.83/77.5 μs) further increases to 176 kA (Fig. 12 (b)). The Y shaped pylon displays a better BFR than Donau and Eagle lattice towers.

VI. Discussion

A. Insulation strength of the optimized pylon

According to the optimization strategy, the detailed down-lead system for this Y shaped pylon has been determined. When the pylon body is a steel mast of 1.5 m radius, there are considerable differences on the structure and insulation strength of the whole pylon compared with the original one. Thus, the insulation characteristics of the pylon need to be verified again. For the optimized pylon, the steel body makes it possible to have a flashover between the tower body and the lower phase conductor. Therefore, potential insulation failures may occur in two regions in Fig. 13: (1) flashover between the shield wire and the upper conductor (U_L), (2) flashover between the lower conductor and the steel pylon body (U_d). In addition, the breakdown at position (2) is the discharge directly from the conductor to the tower mast, which can be treated as an air gap discharge. Therefore, LPM used for air gap [27] can be used to judge whether flashover occurs at position (2). The shortest straight-line distance between lower phase conductor and pylon mast for position (2) is 1.7 m.

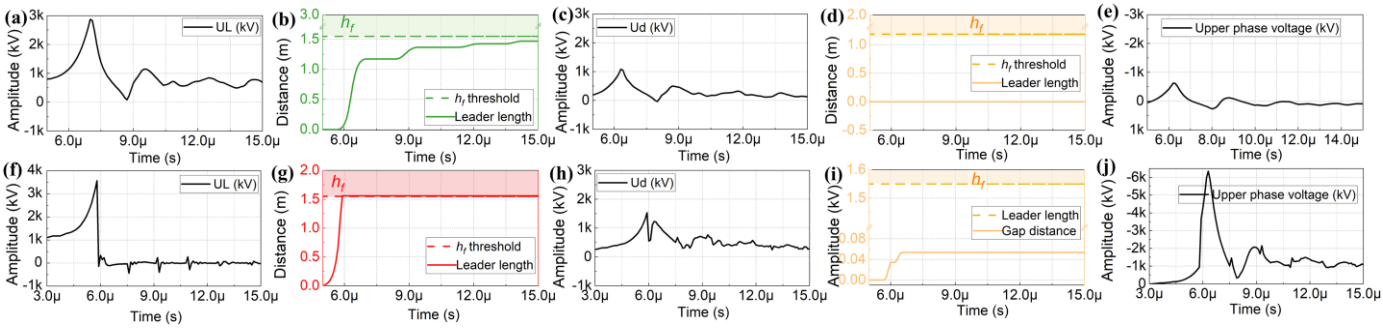

Fig. 14 When striking current is lower than I_c, (a) the U_L waveform, (b) the leader progress length between shield wire and upper phase conductor, (c) the U_d waveform, (d) the leader length in the gap (2), and (e) the upper phase conductor voltage. When the lightning current is 300 kA, (f) the U_L waveform, (g) the leader progress length with time; (h) the U_d waveform, (i) the leader length in the gap (2) with time, and (j) the upper phase voltage when flashover happens. (All the transient voltages response to a lightning current with 3.83/77.5 μs waveform.)

TABLE III
LIGHTNING PERFORMANCE OF Y COMPOSITE PYLON WITH DIFFERENT FORM OF DOWNLEAD, EAGLE AND DONAU TOWERS

Lightning current waveform	ρ_0 (Ω m)	Configuration: Pylon	Configuration: Vertical down-lead	Configuration: Filling materials	I_c (kA) T_f=3.83 μs	$-U_{TT}$ (k kV)	$-U_c$ (k kV)	U_L (k kV)	N_g (flashes /km^2-year)	N_L (flashes /100km-year)	BFR (flashes/100 km-year)	SFFOR (flashes/100 km-year)	LTR (flashes/100 km-year)
CIGRE waveform	100	Y	I I (seperated)	FRP	132	3.27	0.447	2.84	1.39	28.1	0.0238	0	0.0238
			H (connected)		146	3.47	1.15	2.82			0.0118		0.0118
			Cylinder radius of 0.5 (m)	XLPE	162	3.49	0.636	2.85			5.52×10^{-3}		5.52×10^{-3}
			Cylinder radius of 1.5 (m)		176	3.50	0.621	2.88			2.94×10^{-3}		2.94×10^{-3}
		Flashover between down-lead and lower conductor			>300	-	-	-			$<2.38\times10^{-5}$		$<2.38\times10^{-5}$
		Donau			168	3.92	0.52	3.42		38.9	5.75×10^{-3}	0.0234	0.0291
		Eagle			137	3.75	0.399	3.36		41.5	0.0272	0	0.0272

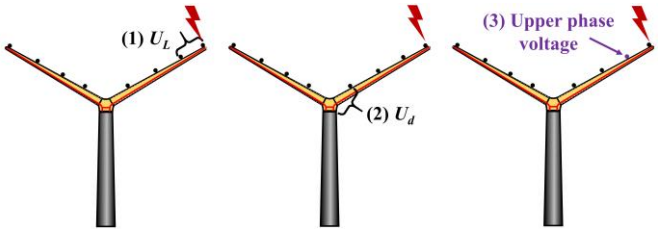

Fig. 13 The overvoltage of interest on the unibody cross-arm: (1) U_L, (2) U_d, (3) upper phase voltage.

When the amplitude of lightning current is not so high as to trigger flashover at region (1) (Fig. 14 (a)). We found that there is no flashover happening at region (2) (Fig. 14 (c)), and Fig. 14 (d) exhibits that there is enough insulation margin in place (2). If the lightning current directly increases to 300 kA, the flashover happens at region (1) (Fig. 14 (f) and (g)). It can be found that the overvoltage in place (2) is slightly increased (Fig. 14 (h)-(i)), but the upper conductor voltage sharply increases to 6300 kV (Fig. 14 (j)). That means when the lightning current exceeds I_c in place (1), the upper conductor provides a path to divert the lighting current from region (1) and the overvoltage in the region (2) is limited to a certain level. Thus, we can conclude that the optimized pylon has enough insulation strength to avoid flashover between the phase conductor and the pylon body.

B. Comparison with traditional towers

Through the method proposed in section II G, BFR for Y shaped pylon with different kinds of T_f are calculated. Besides, we also calculate the BFR of traditional Donau and Eagle towers with same voltage level for comparison. The results are shown in Table III. For 3.83/77.5 μs lightning current waveform, the BFR of Y shaped pylon decreases to 0.00294 flashes/100km-year, which is 12.4 % of the original design.

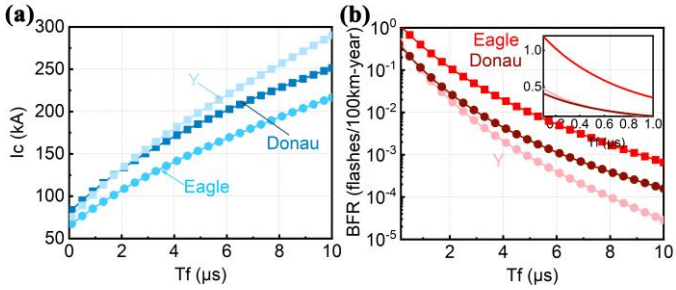

Fig. 15 (a) I_c and (b) BFR corresponding to different T_f for Donau, Eagle, and Y pylons with different T_f.

When we consider a large range T_f (0.2-10 μs), the advantages of insulated towers in lightning protection will be more obvious with the increase of T_f (Fig. 15 (a)), and the BFR decreases exponentially (Fig. 15 (b)). Another index used to indicate the lightning protection level is the lightning trip-out rate (LTR), which refers to all kinds of tripping operation caused by lighting striking, including BFR and shielding failure rate. Reference [8, 9] points out that there is almost no possibility of shielding failure for Eagle tower and Y composite pylon due to the negative protection angle. With the SFFOR taken into consideration, the final LTR for Y shaped pylon and Donau tower are 0.00294 and 0.0291 flashes/100 km-year, and the lightning performance of Y pylon with the optimized down-lead system is much better than that of traditional Donau and Eagle towers.

VII. CONCLUSION

This paper presents the lightning performance of a novel Y shaped pylon with a down-lead going through the cross-arm and pylon body. PSCAD/EMTDC is employed to investigate the transient response of lines when lightning strikes on the top of the pylon. We propose a simplified method to calculate the surge impedance of the inclined down-lead wrapped with insulating materials. Multiple factors that may affect overvoltage including the configuration of down-lead, the span of the pylon, the stroke current propagation speed, and the dielectric constant of filling materials are considered. The research shows that the configuration of the down-lead is major

factor to affect the I_c, but the effect of the filling materials is insignificant. In addition, the current capacity of the down-lead as well as the feasibility of the multi-conductors as the down-lead system is discussed taking the corona effect into consideration. Finally, the implemented pylon grounding system is determined. The XLPE is selected as the filling materials, and the vertical down-lead system is optimized by using a steel mast with expended radius. After optimization, the lightning performance of Y pylon is much better than the traditional Donau and Eagle transmission towers.

APPENDIX

Modeling of lattice towers is expressed in this appendix. The structure parameters of Donau and Eagle tower can be referred in [30]. Multi-story model is employed for tower modeling [27, 39]. For vertical tower body, the surge impedance Z_v can be calculated by equation (6). The surge impedance of the horizontal components such as metal cross-arm and bracing is given as follow [27]

$$Z_h = 60 \ln\left(2h / r_h\right) \tag{27}$$

Where r_h is the radius of horizontal parts. In addition, for the Donau tower, the surge impedance of the tower body is reduced by about 10% by adding the bracings. Thus, the equivalent distributed parameter circuit for the Donau body needs to be connected in parallel with a surge impedance of bracings Z_b, and Z_b=9Z_v [36].

REFERENCES

[1] F. Napolitano, F. Tossani, A. Borghetti and C. A. Nucci, "Lightning Performance Assessment of Power Distribution Lines by Means of Stratified Sampling Monte Carlo Method," *IEEE Trans. Power Deliv.*, vol. 33, no. 5, pp. 2571-2577, Oct. 2018.

[2] W. H. Zhou, Y. B. Wang, R. E. Torres-Olguin, and Z. Chen, "Effect of Reactive Power Characteristic of Offshore Wind Power Plant on Low-Frequency Stability," *IEEE Trans. Energy Convers.*, vol. 35, no. 2, pp. 837-853, Jun. 2020.

[3] E. E. D. f. Consultation, "Ten-Year Network Development Plan 2020. At a glance: Power system needs in 2030 and 2040," 2020.

[4] V. V. Adishchev, A. S. Zubkov, A. I. Ivanov, V. V. Maltsev, A. Y. Panichev, and A. N. Blaznov, "Rational design of steel-GFRP towers for ultracompact overhead power lines," *Mech. Adv. Mater. Struct.*, vol. 27, no. 3, pp. 189-195, Feb. 2020.

[5] Q. Wang, "Experimental investigation on electrical behaviors of an innovative 400-kV double-circuit composite tower," Ph.D. Dissertation, Dept. Enery technol., Aalborg University, Aalborg, Denamrk, 2018.

[6] Q. Wang, C. L. Bak, F. F. da Silva and E. Bystrup, "A state of the art review-methods to evaluate electrical performance of composite cross-arms and composite-based pylons," in *2016 IEEE Electri. Insul. Conf. (EIC)*, 2016, pp. 501-506.

[7] T. Jahangiri, Q. Wang, F. F. da Silva, and C. L. Bak, "Overview of Composite-Based Transmission Pylons," in Electrical Design of a 400 kV Composite Tower: Springer, 2020, pp. 1-13.

[8] T. Jahangiri, C. L. Bak, F. M. F. da Silva, B. Endahl, and J. Holbøll, "Assessment of lightning shielding performance of a 400 kV double-circuit fully composite transmission line pylon," in *CIGRE Int. Counc. Large Electri. Syst.*, 2016, pp. C4-205.

[9] Q. Wang, T. Jahangiri, C. L. Bak, F. F. da Silva, and H. Skouboe, "Investigation on Shielding Failure of a Novel 400-kV Double-Circuit Composite Tower," *IEEE Trans. Power Deliv.*, vol. 33, no. 2, pp. 752-760, Apr. 2018.

[10] Li H, Deng S, Wei Q, et al. "Research on composite material towers used in 110kV overhead transmission lines," in *2010 Int. Conf. High Volt. Eng. Appl*., pp. 572-575, 2010.

[11] Q. Li, S. M. Rowland, and R. Shuttleworth, "Calculating the Surface Potential Gradient of Overhead Line Conductors," *IEEE Trans. Power Deliv*., vol. 30, no. 1, pp. 43-52, Feb. 2015.

[12] Z. G. Datsios, P. N. Mikropoulos, and T. E. Tsovilis, "Effects of Lightning Channel Equivalent Impedance on Lightning Performance of Overhead Transmission Lines," *IEEE Trans. Electromagn. Compat.*, vol. 61, no. 3, pp. 623-630, Jun. 2019.

[13] S. Standards, "Insulation co-ordination – Part 1: Definitions, principles and rules," IEC 60071-1, 2011.

[14] K. O. Papailiou, "Overhead Lines (CIGRE Green Book)", Malters , Switzerland, Springer, 2017, pp. 148-151.

[15] T. Jahangiri, C. L. Bak, F. F. da Silva, and B. Endahl, "Determination of minimum air clearances for a 420kV novel unibody composite cross-arm," in *2015 50th Int. Uni. Power Eng. Conf*., 2015, pp. 1-6.

[16] CIGRE WG C4.407, "Lightning parameters for engineering application," CIGRE Technical Brochure 549, Aug. 2013.

[17] T. Jahangiri, Q. Wang, C. L. Bak, F. F. da Silva, H. J. I. T. O. D. Skouboe, and E. Insulation, "Electric stress computations for designing a novel unibody composite cross-arm using finite element method," *IEEE Trans. Dielectr. Electr. Insul.*, vol. 24, no. 6, pp. 3567-3577, Dec. 2017.

[18] C. Zachariades, S. M. Rowland, I. Cotton, V. Peesapati and D. Chambers, "Development of electric-field stress control devices for a 132 kV insulating cross-arm using finite-element analysis," *IEEE Trans. Power Deliv*., vol. 31, no. 5, pp. 2105-2113, Oct. 2016.

[19] M. Ishii *et al*., "Multistory transmission tower model for lightning surge analysis," *IEEE Trans. Power Deliv.*, vol. 6, no. 3, pp. 1327-1335, Jul. 1991.

[20] M. A. Sargent and M. Darveniza, "Tower surge impedance," *IEEE Trans. Power Appar. Syst.*, vol. PAS-88, no. 5, pp. 680-687, May 1969.

[21] Ghomi, M., Zhang, H., Bak, C.L., da Silva, F.F., and Yin, K., "Integrated Model of Transmission Tower Surge Impedance and Multilayer Grounding System Based on Full-Wave Approach", Elect. Power Syst. Res., vol. 198, p. 107355, Sep. 2021.

[22] A. M. Mousa, "The soil ionization gradient associated with discharge of high currents into concentrated electrodes," *IEEE Trans. Power Deliv.*, vol. 9, no. 3, pp. 1669-1677, Jul. 1994.

[23] A. Yamanaka, N. Nagaoka, Y. Baba, M. Saito and T. Miki, "Lightning Strike to a Tall Grounded Object: Part 1. Circuit Modeling With Direction Dependence," *IEEE Trans. on Electromagn. Compat.*, vol. 61, no. 3, pp. 727-735, Jun. 2019.

[24] J. Gholinezhad and R. Shariatinasab, "Time-domain modeling of tower-footing grounding systems based on impedance matrix," *IEEE Trans. Power Deliv.*, vol. 34, no. 3, pp. 910-918, Jun. 2018.

[25] A. R. Hileman, Insulation coordination for power systems (CRC Press, Boca Raton, Florida), 1999.

[26] B. Wei, Z. Fu and H. Yuan, "Analysis of Lightning Shielding Failure for 500-kV Overhead Transmission Lines Based on an Improved Leader Progression Model," *IEEE Trans. Power Deliv.*, vol. 24, no. 3, pp. 1433-1440, Jul. 2009.

[27] CIGRE WG C4.23, " Procedures for estimating the lightning performance of transmission lines – New aspects," CIGRE Technical Brochure 839, Jun. 2021.

[28] H. Zhang, Q. Wang, F. F. d. Silva, C. L. Bak, K. Yin and H. Skouboe, "Backflashover Performance Evaluation of the Partially Grounded Scheme of Overhead Lines With Fully Composite Pylons," *IEEE Trans. Power Deliv.*, vol. 37, no. 2, pp. 823-832, Apr. 2022.

[29] F. A. M. Rizk, "A model for switching impulse leader inception and breakdown of long air-gaps," *IEEE Trans. Power Deliv.*, vol. 4, no. 1, pp. 596-606, Jan. 1989.

[30] D. Olason, T. Ebdrup, K. Pedersen, F. Da Silva, and C. L. Bak, "A comparison of the lightning performance of the newly designed Eagle pylon and the traditional Donau pylon, based on tower geometry," in *CIGRE Int. Colloq. Lightn. Power Syst.*, 2014.

[31] S. E. Enno, J. Sugier, R. Alber, and M. J. A. R. Seltzer, "Lightning flash density in Europe based on 10 years of ATDnet data," *Atmos. Res.* vol. 235, p. 104769, May 2020.

[32] F. B. Meng et al., "Effect of Thermal Ageing on Physico-Chemical and Electrical Properties of EHVDC XLPE Cable Insulation," *IEEE Trans. Dielectr. Electr. Insul.*, vol. 28, no. 3, pp. 1012-1019, Jun. 2021.

[33] J. Maria, D. Capella, "Study of the behaviour of a n-metal cable screen subject to an adiabatic short-circuit," in *9th Int. Conf. Insul. Power Cables*, p. E5.3, Jun., 2015.

[34] CIGRE Working Group WG 22.12, "The Thermal Behaviour of Overhead Conductors", CIGRE Technical Brochure 207, Aug. 2002.

[35] S. S. M. Ghoneim, M. Ahmed, and N.A. Sabiha, "Transient Thermal Performance of Power Cable Ascertained Using Finite Element Analysis," Processes, vol 9, no. 3, p. 438, Feb. 2021.

[36] Hara T, Yamamoto O. "Modelling of a transmission tower for lightning-surge analysis" *IEE Proceedings-Gener. Transm. Distrib.*,vol 143, no. 3, pp. 283-289, May 1996.

[37] A. J. Aristizábal Cardona, C. A. Páez Chica, and D. H. Ospina Barragán "Behavior and Analysis of the Power System in Steady State". Springer, 2018, pp. 109-118.

[38] M. E. M. Horwitz, S. G. Horwitz, and C. M. Horwitz, "Corona emission and ozone production by carbonized and oxidized high-voltage wires," *IEEE Trans. Power Deliv.*, vol. 21, no. 3, pp. 1636-1640, Jul. 2006.

[39] F. W. Peek, "The Law of Corona and the Dielectric Strength of Air-IV The Mechanism of Corona Formation and Loss," *Trans. Am. Inst. Electr. Eng.*, vol. XLVI, pp. 1009-1024, Jan.-Dec. 1927.